Physica B 407 (2012) 1953–1957

Contents lists available at SciVerse ScienceDirect

Physica B

journal homepage: www.elsevier.com/locate/physb

Strong-coupling electrostatics for two dissimilar charged walls

L. Šamaj [a,b], E. Trizac [b,*]

[a] Institute of Physics, Slovak Academy of Sciences, Dúbravská cesta 9, 84511 Bratislava, Slovakia
[b] Laboratoire de Physique Théorique et Modèles Statistiques, UMR CNRS 8626, Université Paris-Sud, 91405 Orsay, France

ARTICLE INFO

Available online 9 January 2012

Keywords:
Coulomb systems
Strong coupling
Wigner Crystal

ABSTRACT

We study the effective interaction between two parallel charged plates, modelling macromolecules, or colloids, in the strongly coupled Coulomb regime. Neutralizing mobile ions are point-like and confined in the inter-plate slab. A cumulant technique provides exact expansions, beyond the leading strong-coupling order, that are in remarkable agreement with simulation data for both the ionic profile and the inter-plate pressure. The present approach amounts to a summation over relevant excitations around the Wigner Crystal ground state formed at infinite coupling; It thereby differs from previous virial-like strong-coupling theories and generalizes a recent work by the authors to asymmetric plates.

1. Introduction

Experiments in soft matter are often performed in polar solvents such as water, which is also the relevant medium for biological systems. These solvents provide favourable environments for free charges, and macromolecules having dissociable surface groups acquire their solubility from the corresponding solvation effect. Consequently, most organic and inorganic surfaces become charged when immersed in water-like solvents [1–3]. Examples abound, from glass or mica, to nucleic acids or phospholipid membranes.

It has long been realized that the precise ionic distribution of neutralizing counterions around charged macromolecules is the key to understanding the effective interactions between these mesoscopic bodies. The traditional approach to the question leads to the Poisson–Boltzmann description, that has been pioneered a century ago by Gouy and Chapman [4]. It is mean-field in nature, with the neglect of microionic correlations [3,5,6]. Such a framework has proven successful to rationalize experimental findings pertaining to systems where Coulombic couplings – embodied in a to-be defined coupling parameter Ξ – are not too large [2,7]. For highly charged macromolecules and multi-valent microions, the phenomenology nevertheless strongly departs from Poisson–Boltzmann scenario: In particular, it was shown experimentally [8] and by computer simulations [9,10] that similarly charged interfaces can attract under strong coupling (large Ξ), while mean-field predicts repulsion [11–13].

In the last 15 years, the corresponding strong-coupling (SC) regime has witnessed sustained attention [5,6,14–26]. An interesting discussion concerning the length scales at work in the weak-coupling vs strong-coupling dichotomy, can be found in Refs. [3,18,20]. For the sake of the present analysis, we will restrict to charged planar interfaces (the macromolecules), neutralized by point counterions. Remarkably, for large couplings, individual counterions are isolated from each other by their strong mutual repulsion, which creates a marked correlation hole around them. This in turn implies that ionic profiles in the vicinity of one plate or the force between two plates, entirely follow, to leading order in the large coupling parameter Ξ, from a single particle picture where isolated microions experience only the field created by the fixed macromolecule surface charges [3,5,6,14,15]. This phenomenon, that has been extensively assessed by numerical simulations [16,21–23], is also obtained within the field theoretic treatment put forward by Netz and collaborators [16,18–20]. This approach, which amounts to a virial expansion in inverse powers of the coupling constant Ξ, also provides higher order corrections to the leading term. For both the microionic density close to a single plate problem and the two plates pressure, it has been found by comparison with Monte Carlo simulations, that these sub-leading corrections have the right functional form but incorrect prefactors [16,24]. Recently, we have proposed a different strong-coupling expansion technique, that is free of the above shortcomings, and yields excellent agreement when compared to simulation results [24,25]. Our approach is not of the virial type, but stems from considering the relevant excitations of counterions around their ground state positions, that realize a Wigner Crystal. To avoid any confusion between the two different strong-coupling theories, we will coin them “Virial SC” and “Wigner SC”. Our previous publications [24,25] have addressed the symmetric situations where the two interacting charged plates bear the same charge. It is our purpose here to extend the Wigner SC analysis to asymmetric plates, for which Monte Carlo simulation data are available [22]. For such systems, we emphasize that the leading in Ξ behaviour is already known [22,26], but that the sub-leading corrections that will be

* Corresponding author. Tel.: +33 1 69 15 73 39; fax: +33 1 69 15 62 25.

0921-4526/$ - see front matter © 2012 Elsevier B.V. All rights reserved.
doi:10.1016/j.physb.2012.01.073

reported below and that prove important to understand several features observed in the simulations have not been obtained at the virial SC level [18], that was performed in the symmetric case only.

The outline of the paper is as follows. We start in Section 2 by defining the model and useful quantities. Section 3 then presents the cumulant technique used to generate the Wigner SC expansion, from which in particular the force between two unlike charged plates follows. These results are successfully tested against detailed Monte Carlo simulations in Section 4, and conclusions are finally drawn in Section 5.

2. The model: definition and notations

We consider two parallel plates having uniform surface charges $\sigma_1 e$ and $\sigma_2 e$ where e is the elementary charge, the sign of which is immaterial here. The geometry, with an inter-plate distance d, is sketched in the inset of Fig. 1. Mobile counterions of charge $-qe$, constrained to remain in the slab $0\le z\le d$, ensure global electroneutrality. Both situations where $\sigma_1\sigma_2>0$ and $\sigma_1\sigma_2<0$ will be worked out. By appropriate redefinition of parameters, we consider, without loss of generality, that $\sigma_1>0$, $q>0$, and that the asymmetry parameter $\zeta=\sigma_2/\sigma_1$ is in the range $[-1,1]$. We stress that there is always only one type of mobile microion in the system, with charge $-qe$. This means that in the cases $\sigma_1\sigma_2<0$ (so that $\zeta<0$), these microions have a charge of the same sign as plate 2. This also means that at particular asymmetry $\zeta=-1$, the two plate charges balance, and electroneutrality implies that there is no microion present (capacitor limit).

The system is in thermal equilibrium at inverse temperature β. We will work in the framework of the primitive model, where Coulomb interactions only are considered, with a solvent modelled as a dielectric continuum of static permittivity ε. No dielectric discontinuity will be considered (same permittivity in the slab, and outside). Three important length scales characterize the system [3,18,20]. The first is the Bjerrum length $\ell_B=\beta e^2/\varepsilon$, the distance at which two elementary charges' repulsion equals thermal energy β^{-1}. The second is the Gouy length $\mu=1/(2\pi q\ell_B\sigma_1)$ (or equivalently $\mu\zeta$ for plate 2). It measures the typical extension of the ionic profile in the z direction, perpendicular to the interface, when the two plates are at a large distance ($d\to\infty$), both in the weak-coupling and in the strong-coupling limits [27]. The third length is defined in the low temperature limit where the counterions in the vicinity of isolated plate 1 form a hexagonal Wigner Crystal, of lattice spacing $a_\perp=[2q/(\sqrt{3}\sigma_1)]^{1/2}$. From these quantities, the coupling parameter Ξ follows:

$$\Xi=\frac{q^2\ell_B}{\mu}\propto\left(\frac{q^2\ell_B}{a_\perp}\right)^2\propto\left(\frac{a_\perp}{\mu}\right)^2. \tag{1}$$

In the strong-coupling regime defined as the limit of large Ξ, we have $\mu\ll a_\perp\ll q^2\ell_B$.

It will be convenient to introduce dimensionless quantities. Lengths will be made unit-less by normalization with respect to the Gouy length of plate 1: $\tilde z=z/\mu$. Likewise, for the ionic density ρ and inter-plate pressure P, we define dimensionless counterparts

$$\tilde\rho=\frac{\rho}{2\pi\ell_B\sigma_1^2}\quad\text{and}\quad\tilde P=\frac{\beta P}{2\pi\ell_B\sigma_1^2}. \tag{2}$$

Global electroneutrality implies the normalization $\int_0^d dz\,\rho(z)=(\sigma_1+\sigma_2)/q$ or $\int_0^{\tilde d}d\tilde z\,\tilde\rho(\tilde z)=1+\zeta$. On dimensional grounds, the dependence on all parameters can be minimally expressed via the functions $\tilde\rho(\tilde z,\tilde d,\zeta,\Xi)$ and $\tilde P(\tilde d,\zeta,\Xi)$. We will present below a method to obtain explicitly the large Ξ expansions

$$\tilde\rho(\tilde z,\tilde d,\zeta,\Xi)=\tilde\rho_0(\tilde z,\tilde d,\zeta)+\frac{1}{\sqrt{\Xi}}\tilde\rho_1(\tilde z,\tilde d,\zeta)+O\left(\frac{1}{\Xi}\right), \tag{3}$$

$$\tilde P(\tilde d,\zeta,\Xi)=\tilde P_0(\tilde d,\zeta)+\frac{1}{\sqrt{\Xi}}\tilde P_1(\tilde d,\zeta)+O\left(\frac{1}{\Xi}\right), \tag{4}$$

where the leading order terms $\tilde\rho_0$ and $\tilde P_0$ have been obtained in Ref. [22] (see also Ref. [26]). However, before embarking onto the technical analysis, it is useful to remind the contact theorem [28], of particular interest here. It relates the pressure to the microionic densities at contact ($z=0$ or $z=d$), through

$$\tilde P=\tilde\rho(0)-1=\tilde\rho(\tilde d)-\zeta^2. \tag{5}$$

As alluded to above, the case $\zeta=-1$ is trivial: the absence of microions implies that then, $\tilde P=-1$, as it should for a capacitor.

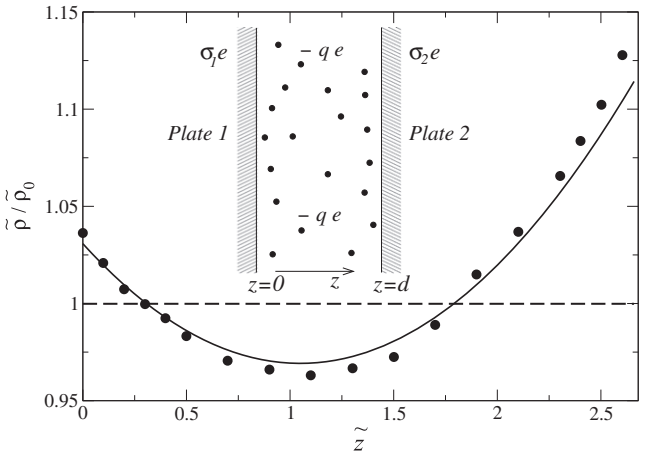

Fig. 1. The filled circles show the density profile measured in the Monte Carlo simulations of Ref. [22], normalized by the leading order term $\tilde\rho_0$ given in Eq. (14). The continuous curve is for our analytical expression (19). Here $\zeta=0.5$, $\Xi=86$, $\tilde d=2.68$. Inset: the two plates geometry considered, where point counterions of charge $-qe$ are confined between two unequally charged parallel plates located at $z=0$ and $z=d$.

3. Wigner SC as a cumulant expansion

The Wigner SC method of Ref. [24] relies on the fact that at infinite coupling $\Xi\to\infty$, counterions form a bilayer Wigner Crystal, collapsing either on the surface at $z=0$ or on the other at $z=d$. At finite but large Ξ, fluctuations of ionic positions around their ground state location start to play a role. Keeping fixed the position of a tagged ion, the idea is to integrate the relevant Boltzmann weight over all other ions' degrees of freedom to compute the density profile. Below, we present a cumulant expansion technique generalizing the approach of Ref. [24] that was essentially heuristic, and as such less adapted to treat the asymmetric case.

In principle, the method supposes that the ground state is known. However, although the main features of the sequence of ground states for symmetric plates with $\zeta=1$, upon varying the inter-plate distance, is available [29], the asymmetric situation is still an open and presumably intricate problem. Indeed, we should expect among other complications, that the local neutrality (which holds for $\zeta=1$) is violated, so that the collapsed microions may overcompensate the charge of plate 1, with a related unbalance on plate 2 [30]. Interestingly, the above difficulties only plague the $\zeta>0$ case, for which they nevertheless become innocuous in the small separation limit. For $\zeta<0$, the charged planar interface 2 and the microions are likely charged, so that the ground state of the system corresponds to a hexagonal

Wigner Crystal on plate 1, with lattice spacing b given by

$$\frac{q}{\sigma_1+\sigma_2}=\frac{\sqrt{3}}{2}b^2. \tag{6}$$

We note that the same structure is necessarily obtained for $d\to 0$ when $\zeta>0$, and more precisely, remains as long as $d\ll b$ (note that b is the two plates counterpart of the length scale $a_\perp$ introduced for one plate in Section 2). In terms of dimensionless quantities, this translates into $\tilde{d}\ll \Xi^{1/2}$. We next treat on equal footing the cases of negative and positive asymmetries ζ, keeping in mind that the resulting expressions will have different ranges of validity.

The aim is to derive the microionic profile from the energy change δE induced by a small shift of particles from the ground state. We denote by $\mathbf{R}_j$ the two-dimensional position of particle j in the ground state, in the direction perpendicular to the z-axis. The third coordinate specifying the ground state position is Z_j which equals 0 or d, depending on the plate on which the ion is collapsed. A small displacement of all particle's positions $\{Z_j\to z_j\}$ translates, up to an irrelevant constant, into

$$-\beta\delta E\simeq -\kappa\sum_{j=1}^{N}\tilde{z}_j+S_z, \tag{7}$$

where $\kappa=1-\zeta=1-\sigma_2/\sigma_1$ and N denotes the number of microions in the system. The first one body term on the rhs stems from the potential created by the walls (it thus vanishes in the symmetric situation $\zeta=1$) while S_z stands for the two body contribution

$$S_z=\frac{3^{3/4}(\sqrt{1+\zeta})^3}{32\pi^{3/2}\sqrt{\Xi}}\sum_{\substack{j,k=1\\(j\neq k)}}^{N}\frac{(\tilde{z}_j-\tilde{z}_k)^2}{(|\mathbf{R}_j-\mathbf{R}_k|/b)^3}. \tag{8}$$

For large Ξ, S_z is a perturbation to the one body term, that is here truncated to harmonic order. Higher order contributions in the set $\{z_j\}$ can be computed, together with the contributions from shifts $\delta\mathbf{R}_j$ along the plates; they turn out, however, to be sub-dominant compared to the harmonic in z terms retained in Eq. (8) [31], and irrelevant to compute the first two terms of the expansions (3) and (4). It should be noted here that S_z of course bears the signature of the ground state, but only through the "parallel" projected positions $\mathbf{R}_j$, as opposed to the perpendicular coordinate Z_j.

The particle density at a given point $\mathbf{r}$ can be defined as $\rho(\mathbf{r})=\langle\sum_{j=1}^{N}\delta(\mathbf{r}-\mathbf{r}_j)\rangle$ where the statistical average is performed with weight $\exp(-\beta\delta E)$. For explicit calculations, it is convenient to introduce a generating potential $u(\mathbf{r})$, that is an auxiliary quantity to be set to 0 *in fine*. In doing so, the partition function of our system reads

$$Z_N[w]=\frac{1}{N!}\int_{\Lambda}\prod_{j=1}^{N}[d\mathbf{r}_i\, w(\mathbf{r}_i)e^{-\kappa\tilde{z}_i}]\exp(S_z), \tag{9}$$

where Λ denotes the integration region, i.e. the slab $\{0\le z_i\le d\}$. From the partition function and the generating Boltzmann weight $w(\mathbf{r})=\exp[-\beta u(\mathbf{r})]$, we obtain the particle density as the functional derivative

$$\rho(\mathbf{r})=\frac{\delta}{\delta w(\mathbf{r})}\ln Z_N[w]\Big|_{w(\mathbf{r})=1}. \tag{10}$$

To treat S_z perturbatively, we need to introduce the non-interacting counterpart of $Z_N[w]$,

$$Z_N^{(0)}[w]=\frac{1}{N!}\int_{\Lambda}\prod_{j=1}^{N}[d\mathbf{r}_i w(\mathbf{r}_i)e^{-\kappa\tilde{z}_i}]=\frac{1}{N!}\left[\int_{\Lambda}d\mathbf{r}w(\mathbf{r})e^{-\kappa\tilde{z}}\right]^N, \tag{11}$$

and consistently, the non-interacting statistical average $\langle\cdots\rangle_0$. From these very definitions, we have $Z_N[w]=Z_N^{(0)}[w]\langle\exp(S_z)\rangle_0$. Inserting this relation into Eq. (10), it appears that the leading SC contribution ρ_0 is associated to $\ln Z_N^{(0)}[w]$, whereas the sub-leading term ρ_1 follows from the functional derivative of $\ln\langle\exp(S_z)\rangle_0$. The latter expression is eligible for a cumulant expansion in the form

$$\ln\langle\exp(S_z)\rangle_0=\sum_{n=1}^{\infty}\frac{1}{n!}\langle S_z^n\rangle_0^{(c)}=\langle S_z\rangle_0+\frac{1}{2}(\langle S_z^2\rangle_0-\langle S_z\rangle_0^2)+\cdots, \tag{12}$$

where for the sake of our purposes, it is sufficient to truncate the expansion at first order. Higher order terms contribute to higher powers in $1/\Xi$ in Eqs. (3) and (4). Writing $\ln Z_N[w]\simeq\ln Z_N^{(0)}[w]+\langle S_z\rangle_0$ our task is now to compute the functional derivative appearing in Eq. (10).

We start with the leading SC term

$$\rho_0(\mathbf{r})=\frac{\delta}{\delta w(\mathbf{r})}\ln Z_N^{(0)}[w]\Big|_{w(\mathbf{r})=1}=\frac{Ne^{-\kappa\tilde{z}}}{\int_{\Lambda}d\mathbf{r}e^{-\kappa\tilde{z}}}. \tag{13}$$

In dimensionless form, this yields

$$\tilde{\rho}_0(\tilde{z},\tilde{d},\zeta)=(1-\zeta^2)\frac{e^{-\kappa\tilde{z}}}{1-e^{-\kappa\tilde{d}}}, \tag{14}$$

which is the form already reported in Ref. [22], as it should; it expresses the fact that to leading order, the profile adapts to the potential created by the plates only (single particle picture), while microionic correlation embodied in S_z turn into the sub-leading correction to $\tilde{\rho}_0$. In the symmetric limit $\zeta\to 1$, Eq. (14) gives a flat profile $\tilde{\rho}_0=2/\tilde{d}$, which is indeed the correct result [16,20,24].

The first sub-leading correction stems from $\langle S_z\rangle_0$ which involves averages of the form $\langle\tilde{z}_j\tilde{z}_k\rangle_0$. For $j\neq k$, the above average decouples into $\langle\tilde{z}_j\rangle_0\langle\tilde{z}_k\rangle_0$ due to particles' independence. In addition

$$\langle\tilde{z}_j^p\rangle_0=\frac{\int_{\Lambda}\prod_{i=1}^{N}[d\mathbf{r}_i\, w(\mathbf{r}_i)e^{-\kappa\tilde{z}_i}]\tilde{z}_j^p}{\int_{\Lambda}\prod_{i=1}^{N}[d\mathbf{r}_i\, w(\mathbf{r}_i)e^{-\kappa\tilde{z}_i}]}=\frac{\int_{\Lambda}d\mathbf{r}\, w(\mathbf{r})e^{-\kappa\tilde{z}}\tilde{z}^p}{\int_{\Lambda}d\mathbf{r}\, w(\mathbf{r})e^{-\kappa\tilde{z}}}\equiv\langle\tilde{z}^p\rangle_0 \tag{15}$$

does not depend on the particle's index j, so that upon averaging Eq. (8), we have

$$\langle S_z\rangle_0=\frac{3^{3/4}(\sqrt{1+\zeta})^3}{16\pi^{3/2}\sqrt{\Xi}}NC_3[\langle\tilde{z}^2\rangle_0-\langle\tilde{z}\rangle_0^2], \tag{16}$$

where C_3 is a signature of the ground state structure. For a hexagonal Wigner Crystal, C_3 reads

$$C_3=\sum_{\substack{j,k=-\infty\\(j,k)\neq(0,0)}}^{\infty}\frac{1}{(j^2+jk+k^2)^{3/2}}=\frac{2}{\sqrt{3}}\zeta\left(\frac{3}{2}\right)\left[\zeta\left(\frac{3}{2},\frac{1}{3}\right)-\zeta\left(\frac{3}{2},\frac{2}{3}\right)\right] \tag{17}$$

with $\zeta(z,q)=\sum_{n=0}^{\infty}1/(q+n)^z$ the generalized Riemann zeta function and $\zeta(z)\equiv\zeta(z,1)$, which should not be confused with the asymmetry parameter ζ. Numerical evaluation gives $C_3=11.034\ldots$. The final step of the calculation requires

$$\frac{\delta\langle\tilde{z}^p\rangle}{\delta w(\mathbf{r})}\Big|_{w(\mathbf{r})=1}=\frac{e^{-\kappa\tilde{z}}}{\int_{\Lambda}d\mathbf{r}e^{-\kappa\tilde{z}}}\left(\tilde{z}^p-\frac{\int_{\Lambda}d\mathbf{r}\,\tilde{z}^p e^{-\kappa\tilde{z}}}{\int_{\Lambda}d\mathbf{r}\,e^{-\kappa\tilde{z}}}\right) \tag{18}$$

for $p=1$ and $p=2$, from which, making use of Eq. (16), $\delta\langle S_z\rangle_0/\delta w(\mathbf{r})|_{w=1}$ ensues. Gathering results, we obtain the density profile

$$\tilde{\rho}(\tilde{z})=(1-\zeta^2)\frac{e^{-\kappa\tilde{z}}}{1-e^{-\kappa\tilde{d}}}\left\{1+\frac{(3^{1/4}\sqrt{1+\zeta})^3C_3}{16\pi^{3/2}\sqrt{\Xi}}\times[\tilde{z}^2-t_2-2t_1(\tilde{z}-t_1)]+O\left(\frac{1}{\Xi}\right)\right\}, \tag{19}$$

where

$$t_1(\kappa)=\frac{1}{\kappa}-\frac{\tilde{d}}{e^{\kappa\tilde{d}}-1}, \tag{20}$$

$$t_2(\kappa)=\frac{2}{\kappa^2}-\frac{1}{e^{\kappa\tilde{d}}-1}\left(\frac{2\tilde{d}}{\kappa}+\tilde{d}^2\right). \tag{21}$$

The two contributions appearing in Eq. (3) can be directly read in Eq. (19). The first one is $\tilde{\rho}_0$, as given by Eq. (14), and we can check that the second, sub-leading term is well behaved in the symmetric limit $\zeta\to 1$, where it reduces to the result obtained in Ref. [24]. Indeed, for $\kappa\to 0$, we have $t_1\to\tilde{d}/2$, $t_2\to\tilde{d}^2/3$, and

$$\tilde{\rho}(\tilde{z})=\frac{2}{\tilde{d}}+\frac{3^{3/4}C_3\sqrt{2}}{8\pi^{3/2}\sqrt{\Xi}}\frac{1}{\tilde{d}}\left[\left(\tilde{z}-\frac{\tilde{d}}{2}\right)^2-\frac{\tilde{d}^2}{12}\right]. \tag{22}$$

The next terms in this expansion are of order $1/\Xi$.

It is interesting to check that the general expression (19) fulfills the contact theorem (5), which imposes that $\tilde{\rho}(0)-\tilde{\rho}(\tilde{d})=1-\zeta^2$, for all charge asymmetries and inter-plate distance. This self-consistency test is rather stringent, and ensures that the same pressure follows from applying the contact theorem at $z=0$ or $z=d$, as it should. The explicit expression can be written $\tilde{P}=\tilde{P}_0+\tilde{P}_1/\sqrt{\Xi}+O(1/\Xi)$ as in Eq. (4), where

$$\tilde{P}_0=-\frac{1}{2}(1+\zeta^2)+\frac{1}{2}(1-\zeta^2)\coth\left(\frac{1-\zeta}{2}\tilde{d}\right) \tag{23}$$

is the leading SC contribution, already obtained within the virial SC method in Ref. [22], and

$$\tilde{P}_1=\frac{3^{3/4}(1+\zeta)^{5/2}C_3}{4(4\pi)^{3/2}}\frac{\tilde{d}}{\sinh^2\left(\frac{1-\zeta}{2}\tilde{d}\right)}\left[\left(\frac{1-\zeta}{2}\tilde{d}\right)\coth\left(\frac{1-\zeta}{2}\tilde{d}\right)-1\right] \tag{24}$$

is the coefficient of the first $1/\sqrt{\Xi}$ correction.

4. Discussion and comparison to Monte Carlo simulations

By construction, the explicit expressions obtained in Section 3 for the density profile and the pressure are valid as long as the ground state of the system is close to the hexagonal structure assumed, which sets the precise value of C_3. As alluded to above, we therefore expect that our expressions should provide the correct leading plus first order correction results for all distances d when $\zeta<0$, while for the more physically relevant case of positive charge ratio ($\zeta>0$), the condition $d\ll b$ (or equivalently $\tilde{d}\ll\sqrt{\Xi}$) should be enforced. Consistently, we note that while $\tilde{P}_1$ vanishes for large d, $\tilde{P}_0\to-\zeta^2$ in the same limit. Such a result is correct for $\zeta<0$, where for large d, all microions are expelled from the vicinity of the like-charged plate 2, implying $\tilde{\rho}(\tilde{d})\to 0$, and hence $\tilde{P}\to-\zeta^2$ from the contact theorem. On the other hand, for $\zeta>0$, the two plates decouple when d becomes large, so that the pressure then vanishes. Clearly, our expressions do not cover the large d limit in cases $\zeta>0$.

To assess the validity of our approach, we turn to a comparison with Monte Carlo simulations, performed for the same system of point counterions between two unequally charged plates in Ref. [22]. It can be seen in Fig. 1 for $\zeta=0.5$, that already at $\Xi=86$, which is not a particularly high value, Eq. (19) captures the subtleties of the deviations from the leading order term $\tilde{\rho}_0$. An equally good agreement is found for the case $\zeta=0$ also studied in Ref. [22], and for the pressure, under the proviso $\tilde{d}\ll\sqrt{\Xi}$ for $\zeta>0$. We mention here that the situations of negative asymmetries have received less attention in the numerical investigations than the case $\zeta>0$. An interesting question that finds an answer in our analysis lies in the fate of the like-charge attraction phenomenon when Ξ and ζ are changed. From Eqs. (23) and (24), it is simple to identify the values of $\tilde{P}$ which discriminate the attractive ($\tilde{P}<0$) from the repulsive ($\tilde{P}>0$) regimes. In doing so, Fig. 2 indicates

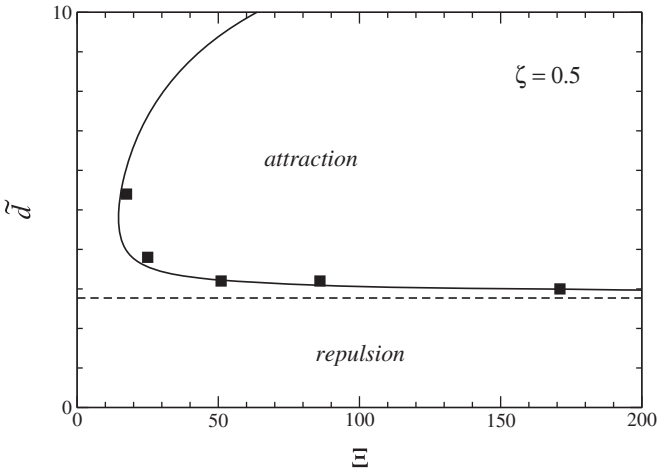

Fig. 2. Phase-diagram for like-charged plates with charge asymmetry $\zeta=\sigma_2/\sigma_1=0.5$. The squares come from the Monte Carlo results [22], and the continuous curve is the locus of points where the pressure given by Eqs. (23) and (24) vanishes. The dashed line follows from the leading order approximation $\tilde{P}=\tilde{P}_0$.

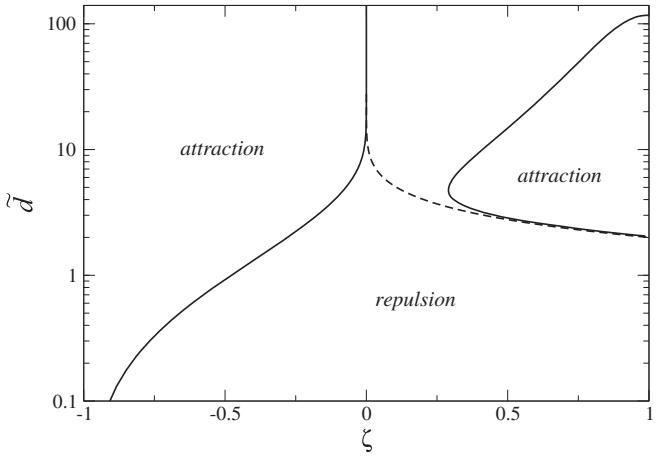

Fig. 3. Phase behaviour at $\Xi=10^3$ as a function of charge asymmetry. The continuous curve shows where the pressure given by (23) and (24) vanishes, and the dashed line corresponds to the leading-order result where $\tilde{P}_0=0$, for which it is found that $\tilde{d}=-2(\ln|\zeta|)/(1-\zeta)$ [22]. For $\zeta<0$ the dashed and continuous curves are practically indistinguishable.

that we fully capture the features observed numerically, at variance with the previously derived leading SC approximation. It is also instructive to sketch the phase diagram for a given coupling parameter, as the asymmetry ζ is changed (see Fig. 3).It appears that while sub-leading corrections do not significantly affect the negative ζ part of the phase diagram, they significantly distort the other moiety. Indeed, for $\Xi=10^3$, no-like charge attraction is found in the range $0<\zeta<0.29$, whereas the leading-order approximation predicts such an effect for all ζ (see the dashed line).

5. Conclusion

Within a statistical mechanics cumulant expansion framework, we have derived the counterion density profiles and pressure between two planar uniformly charged walls, in the limit of strong Coulombic coupling Ξ. Compared to previous works, we have addressed the asymmetric situation where the

charge ratio between both plates $\zeta = \sigma_2/\sigma_1$ is arbitrary in magnitude and in sign. Our results recover previously obtained Wigner strong-coupling (SC) calculations for symmetric plates [24], and are found in excellent agreement with Monte Carlo simulation data. In this, they significantly improve upon previously proposed virial SC approaches [3,16,22]. We have shown in particular that the sub-leading correction to the dominant SC order fundamentally affects the phase boundaries of the like-charge attraction phase diagram. Investigations on curved macromolecules, with or without dielectric inhomogeneities, provide interesting venues for future work.

Acknowledgements

We acknowledge the support received from the grants VEGA No. 2/0049/12 and CE-SAS QUTE.

References

[1] J.-P. Hansen, H. Löwen, Annu. Rev. Phys. Chem. 51 (2000) 209.
[2] L. Belloni, J. Phys.: Condens. Matter 12 (2000) 549.
[3] A. Naji, M. Kanduč, R.R. Netz, R. Podgornik, in: D. Andelman, G. Reiter (Eds.), Understanding Soft Condensed Matter via Modeling and Computation, Addison Wesley, 2010.
[4] G. Gouy, J. Phys. (Paris) 9 (1910) 457;
D.L. Chapman, Philos. Mag. 25 (1913) 475.
[5] A.Y. Grosberg, T.T. Nguyen, B.I. Shklovskii, Rev. Mod. Phys. 74 (2002) 329.
[6] Y. Levin, Rep. Prog. Phys. 65 (2002) 1577.
[7] R.J. Hunter, Foundations of Colloid Science, 2nd ed., Oxford University Press, 2005.
[8] A. Khan, B. Jönsson, H. Wennerström, J. Phys. Chem. 89 (1985) 5180;
R. Kjellander, S. Marcelja, J.P. Quirk, J. Colloid Interface Sci. 126 (1988) 194;
M. Dubois, T. Zemb, N. Fuller, R.P. Rand, V.A. Parsegian, J. Chem. Phys. 108 (1998) 7855.
[9] L. Guldbrand, B. Jönson, H. Wennerström, P. Linse, J. Chem. Phys. 80 (1984) 2221;
D. Bratko, B. Jönsson, H. Wennerström, Chem. Phys. Lett. 128 (1986) 449.
[10] R. Kjellander, Ber. Bunsenges. Phys. Chem. 100 (1996) 894.
[11] J.C. Neu, Phys. Rev. Lett. 82 (1999) 1072.
[12] J.E. Sader, D.Y. Chan, J. Colloid Interface Sci. 213 (1999) 268;
J.E. Sader, D.Y. Chan, Langmuir 16 (2000) 324.
[13] E. Trizac, Phys. Rev. E 62 (2000) R1465.
[14] I. Rouzina, V.A. Bloomfield, J. Phys. Chem. 100 (1996) 9977.
[15] V.I. Perel, B.I. Shklovskii, Physica A 274 (1999) 446;
B.I. Shklovskii, Phys. Rev. E 60 (1999) 5802.
[16] A.G. Moreira, R.R. Netz, Europhys. Lett. 52 (2000) 705;
A.G. Moreira, R.R. Netz, Phys. Rev. Lett. 87 (2001) 078301;
A.G. Moreira, R.R. Netz, Eur. Phys. J. E 8 (2002) 33.
[17] A.W.C. Lau, D. Levine, P. Pincus, Phys. Rev. Lett. 84 (2000) 4116;
A.W.C. Lau, P. Pincus, D. Levine, H.A. Fertig, Phys. Rev. E 63 (2001) 051604.
[18] R.R. Netz, Eur. Phys. J. E 5 (2001) 557.
[19] H. Boroudjerdi, Y.-W. Kim, A. Naji, R.R. Netz, X. Schlagberger, A. Serr, Phys. Rep. 416 (2005) 129.
[20] A. Naji, S. Jungblut, A.G. Moreira, R.R. Netz, Physica A 352 (2005) 131.
[21] Y.S. Jho, M. Kanduč, A. Naji, R. Podgornik, M.W. Kim, P.A. Pincus, Phys. Rev. Lett. 101 (2008) 188101.
[22] M. Kanduč, M. Trulsson, A. Naji, Y. Burak, J. Forsman, R. Podgornik, Phys. Rev. E 78 (2008) 061105.
[23] D.S. Dean, R.R. Horgan, A. Naji, R. Podgornik, J. Chem. Phys. 130 (2009) 094504.
[24] L. Šamaj, E. Trizac, Phys. Rev. Lett. 106 (2011) 078301.
[25] L. Šamaj, E. Trizac, Eur. Phys. J. E 34 (2011) 20.
[26] F. Paillusson, E. Trizac, Phys. Rev. E 84 (2011) 011407.
[27] R. Messina, J. Phys.: Condens. Matter 21 (2009) 113102.
[28] D. Henderson, L. Blum, J.L. Lebowitz, J. Electroanal. Chem. 102 (1979) 315;
S.L. Carnie, D.Y.C. Chan, J. Chem. Phys. 74 (1981) 1293;
H. Wennerström, B. Jönsson, P. Linse, J. Chem. Phys. 76 (1982) 4665.
[29] G. Goldoni, F.M. Peeters, Phys. Rev. B 53 (1996) 4591;
R. Messina, H. Löwen, Phys. Rev. Lett. 91 (2003) 146101;
V. Lobaskin, R.R. Netz, Europhys. Lett. 77 (2007) 38003.
[30] R. Messina, C. Holm, K. Kremer, Phys. Rev. Lett. 85 (2000) 872.
[31] L. Šamaj, E. Trizac, Phys. Rev. E 84 (2011) 041401.